


Controllable three-dimensional electrostatic lattices for manipulation of cold polar moleculesHengjiao Guo, Yabing Ji , Qing Liu, Tao Yang, Shunyong Hou,^{*} and Jianping Yin[†]*State Key Laboratory of Precision Spectroscopy, East China Normal University, Shanghai 200062, China*

(Received 13 December 2021; accepted 20 April 2022; published 10 May 2022)

Engineering many-body systems of particles in lattices has attracted intense interest in the last few decades, thanks to their promising applications such as in quantum computation or topological matter. While lattices of different dimensions have been demonstrated with magnetic and/or optical fields, little work has been done upon three-dimensional (3D) electrostatic lattices to tame polar molecules. Here, we propose a 3D electrostatic lattice consisting of periodically distributed square-patterned electrodes in space, whose potentials reach tens of millikelvin and can be controlled easily. Detailed analysis and Monte Carlo simulations indicate that ND_3 molecules in its $|J, KM\rangle = |1, -1\rangle$ state can be effectively trapped and evaporatively cooled. In addition, replacing the electrodes with different patterns enables realizing 3D electric lattices with new topological geometry (e.g., honeycomb or kagome). As a natural extension of the 3D optical and magnetic lattices, the 3D electrostatic lattice offers intriguing perspectives for cold chemistry, quantum simulation, and precision metrology.

DOI: [10.1103/PhysRevA.105.053108](https://doi.org/10.1103/PhysRevA.105.053108)**I. INTRODUCTION**

Lattice, characteristic of hundreds of potential traps and small sizes, serves as a convenient platform for taming a single particle or many-body system. Atomic lattice has been pursued for decades due to its intriguing prospects in fields including but not limited to condensed-matter physics and quantum information processing [1,2]. For instance, engineering many-body systems of ultracold quantum gases in three-dimensional (3D) optical lattice enables one to gain insights into complex solid-state systems, leading to the discovery of “artificial crystal of light” [3]. In addition, magnetic or magneto-optical lattices for cold atoms have also been demonstrated and widely utilized in atomic matter wave interference [4,5] and Mott insulator quantum phase transition [6].

The complicated internal energy level structure of molecules, on one hand, offers enhanced sensitivity in precision spectroscopy and measurement in fundamental physics, but on the other hand, brings great difficulties to realize molecular cooling and trapping. In the last two decades, experimental techniques that produce intense cold molecular gases have been invented, which we can divide into four categories in general. (i) Deceleration (filtering) methods utilizing conservative fields including electric [7–9], magnetic [10,11], or laser fields [12] to slow down (filter) molecular beams produced from a jet (reservoir) to get slow-moving molecules. (ii) Laser cooling methods employ the dissipative force from laser to chill certain molecules that depict the quasiclosed cycling scheme in the molecular schemes [13]. (iii) Collision techniques such as evaporative cooling [14], sympathetic cooling [15], and buffer gas cooling [16] that are achieved by

elastic collisions between molecules or atoms. (iv) Synthetic methods using magnetic [17,18] and/or laser light [19,20] to generate ultracold molecules from ultracold atoms, which is a prevalent way to prepare a quantum degenerate molecular gas. The combination of molecular cooling and lattices gives rise to a wealth of opportunities in fundamental physics, precision metrology, and quantum computation. Recently, evaporative cooling of chemically active molecules was demonstrated in optical lattices, which paved the way for the study of collective quantum many-body physics [14].

While a great number of excellent studies on one-dimensional [21,22] and two-dimensional (2D) [23,24] electrostatic lattices for polar molecules were conducted, little work on the 3D electrostatic lattice is not readily available, mostly due to the complex energy level structure of cold polar molecules. Here, we propose a design of a 3D electrostatic lattice for cold polar molecules based on the following considerations. First, the 3D electrostatic lattice is suited to tame polar molecules, and is a natural extension of the 3D optical and the 3D magnetic (-optical) lattices. Second, the depth of 3D electrostatic lattices is typically several orders of magnitude deeper than that of 3D optical lattices, thus allowing for powerful control of polar molecules over comparatively large energy scales. Third, by replacing the electrodes with different patterns, our scheme enables realizing 3D electric lattices with various topological geometries such as quadrilateral, honeycomb, or kagome. Furthermore, the voltage on each electrode can be controlled individually, thus enabling both tunability of local electric field distribution and generation of uneven lattice patterns for exotic topological band structures.

In this paper, we first focus on the design of the 3D electric lattice scheme as well as a detailed theoretical analysis. The molecular trajectory calculations are then carried out to simulate the molecular trapping and evaporative cooling processes.

^{*}Corresponding author: syhou@lps.ecnu.edu.cn[†]Corresponding author: jpyin@phy.ecnu.edu.cn

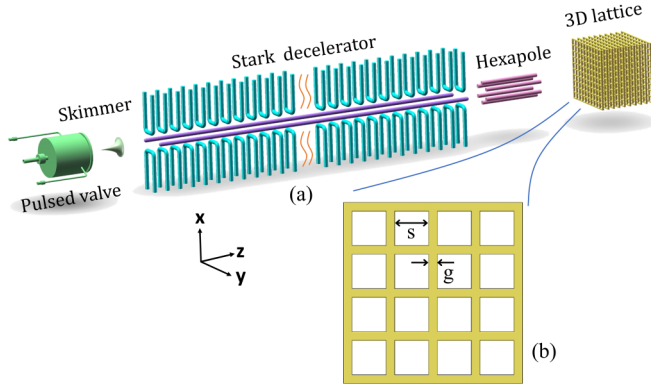


FIG. 1. (a) Schematic view of the 3D electrostatic lattice for trapping a Stark-decelerated cold polar molecular beam. The 3D electrostatic lattice is formed by a series of periodically spaced electrode plates. (b) Zoom-in view of one piece of plate of the 3D electric lattice, together with the pattern parameters.

Some possible topological geometries and applications of the 3D electric lattice are also discussed.

II. LATTICE DESIGN AND THEORETICAL ANALYSIS

Figure 1(a) depicts an application scenario of our designed 3D electrostatic lattice in a cold molecular experiment, where the electrostatic lattice is located close to the end of a Stark decelerator [25]. A supersonic beam produced by a pulsed valve [26,27] is slowed down via the Stark decelerator and then coupled into the 3D electrostatic lattice. The lattice is composed of thin metal electrode plates with a square hole array. Figure 1(b) presents a detailed view of one electrode plate of the lattice. These plates have a thickness of c and are evenly spaced with a distance of d . The length of the square hole on the plate is s and the width of the metal frame between two square holes is g . By applying appropriate voltages on these metal plates, a 3D electric potential array can be formed among the metal plate array. The longitudinal (along the z axis) and transverse (x or y axis) periodicity of the 3D electrostatic lattice is Nd and $s + g$, respectively, in which N indicates the number of electrodes in one longitudinal periodicity.

One can express the fixed voltage applied on each electrode as the following expression:

$$V_n = V_0 \sin\left(\phi_0 + \frac{2\pi n}{N}\right), \quad (1)$$

where V_0 is the voltage amplitude, ϕ_0 is the phase offset, and n is the electrode index number. In the following discussion, the voltage of lattice refers to the voltage amplitude V_0 . The parameters of the 3D lattice are set as follows: $d = 40 \mu\text{m}$, $c = g = 10 \mu\text{m}$, $s = 50 \mu\text{m}$, and $N = 8$. Therefore, the longitudinal and transverse periodicity of the 3D lattice is 320 and $60 \mu\text{m}$. One can find that there are two electric field minima in one longitudinal period. That is to say, the distance of the neighboring electric traps in the longitudinal direction is $160 \mu\text{m}$. It should also be noted that the geometries of the electrode plates are subject to scaling up or down if needed.

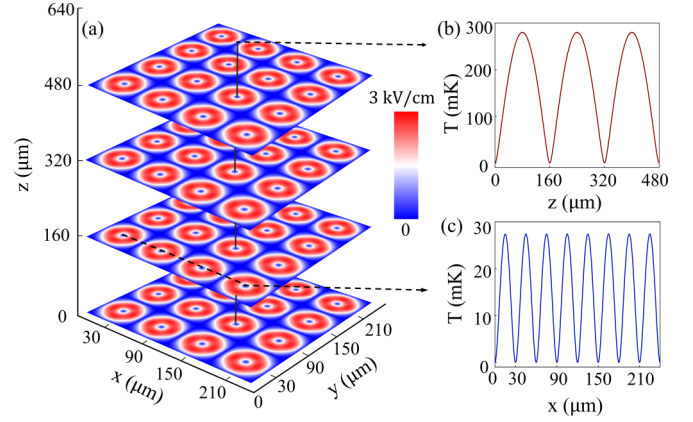


FIG. 2. Four slices of the electric field distributions of the 3D electrostatic lattice at different positions through the electric field minima of the sites (a), together with the potential-well distribution along the longitudinal (b) and the lateral (c) directions for ND_3 molecules.

The electric potential $\phi(x, y, z)$ in the electric lattice can then be expressed as

$$\begin{aligned} \phi(x, y, z) = & \sum_{m,n,l} A_{mnl} [\cos(mk_x x + \phi_1) + \sin(mk_x x + \phi_1)] \\ & \times [\cos(nk_y y + \phi_1) + \sin(nk_y y + \phi_1)] \\ & \times [\cos(lk_z z + \phi_2) + \sin(lk_z z + \phi_2)], \quad (2) \end{aligned}$$

where $k_x = k_y = \frac{2\pi}{L_1}$, $k_z = \frac{2\pi}{L_2}$, and L_1 and L_2 are the periodicity of potential in the transverse and longitudinal direction, respectively. According to the parameter settings mentioned above, $L_1 = 60 \mu\text{m}$, $L_2 = 320 \mu\text{m}$, $\phi_1 = \frac{\pi}{4}$, and $\phi_2 = -\frac{\pi}{8}$. When taking $m, n, l = 0, 1, 2$, the coefficients A_{mnl} can be obtained by comparing each Fourier component with Eq. (2), using the method similar to Ref. [28]. Once the potential $\phi(x, y, z)$ is determined, the electric fields can be given by the following equation:

$$E_i = \frac{\partial \phi}{\partial i}, \quad (3)$$

with $i = x, y, z$. Then the magnitude of the electric field in the lattice is achieved with

$$|\vec{E}| = \sqrt{(E_x)^2 + (E_y)^2 + (E_z)^2}. \quad (4)$$

The resulting electric field distributions can be derived based on Eqs. (2)–(4), as shown in Fig. 2(a). It shows four slices of the electric field distributions in the x - y planes through the minima of the lattice sites, which are in the right middle of two neighboring plates. Each slice in Fig. 2(a) is patterned with a 2D potential array, with separations of 60 and $160 \mu\text{m}$ in the lateral (x or y axis) and the longitudinal (z axis) directions, respectively. Figure 2(b) shows the electric field distribution of the 3D lattice at different positions through the electric field minima of the sites. When V_0 is set to 100 V , the trap depth for ND_3 molecules in the $|J, KM\rangle = |1, -1\rangle$ state reaches 27.5 and 280 mK in the lateral and longitudinal directions, respectively. Here M and K are the projections of the total angular momentum \vec{J} on the electric field \vec{E} and along

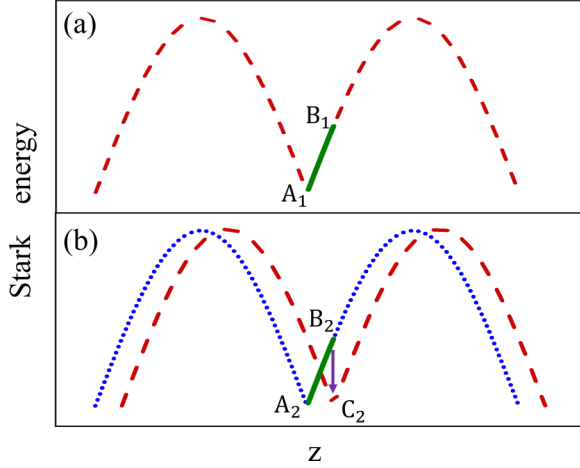


FIG. 3. Loading and trapping polar molecules into the 3D electric lattice employing only one electric field configuration (a) and two different electric field configurations in succession (b). The dashed red line and dotted blue line represent the Stark potential energy of the molecules in the lattice, and the solid green lines indicate the molecular potential energy gained in the loading processes.

the symmetry axis, respectively. As visualized in Fig. 2, a 3D electrostatic lattice with a certain configuration can be formed for polar molecules prepared in low-field-seeking states.

The force felt by a polar molecule in electric fields is given by

$$\begin{Bmatrix} F_x \\ F_y \\ F_z \end{Bmatrix} = - \left(\frac{1}{|\vec{E}|} \frac{dW}{d|\vec{E}|} \right) \begin{Bmatrix} \frac{\partial^2 \phi}{\partial x^2} & \frac{\partial^2 \phi}{\partial x \partial y} & \frac{\partial^2 \phi}{\partial x \partial z} \\ \frac{\partial^2 \phi}{\partial x \partial y} & \frac{\partial^2 \phi}{\partial y^2} & \frac{\partial^2 \phi}{\partial y \partial z} \\ \frac{\partial^2 \phi}{\partial x \partial z} & \frac{\partial^2 \phi}{\partial y \partial z} & \frac{\partial^2 \phi}{\partial z^2} \end{Bmatrix} \begin{Bmatrix} \frac{\partial \phi}{\partial x} \\ \frac{\partial \phi}{\partial y} \\ \frac{\partial \phi}{\partial z} \end{Bmatrix} \quad (5)$$

For ND_3 molecules in the $|J, KM\rangle = |1, -1\rangle$ state, the Stark potential $W(|\vec{E}|)$ can be expressed as

$$W(|\vec{E}|) = \pm \sqrt{\left(\frac{W_{\text{inv}}}{2} \right)^2 + (\mu_{\text{eff}} |\vec{E}|)^2} - \frac{W_{\text{inv}}}{2}, \quad (6)$$

where $W_{\text{inv}} = 0.053 \text{ cm}^{-1}$ is the zero-field inversion splitting and μ_{eff} is the effective dipole moment with the expression $\mu_{\text{eff}} = \mu MK/[J(J+1)]$. Here, $\mu = 1.5 \text{ D}$ is the permanent electric dipole moment of the ND_3 molecule.

III. TRAPPING AND EVAPORATIVE COOLING

A. Loading and trapping

The 3D electric lattice can be filled with slow-moving polar molecules produced by, for example, Stark deceleration or bend filtering. The loading efficiency of molecules into the 3D lattice is key for the subsequent molecular experiments. We employ a so-called ‘‘synchronous molecule’’ for convenience in describing the operation sequence, which is a virtual molecule moving along the beam axis and always synchronized with the change of the external electric field. There are two different loading methods for our designed 3D electrostatic lattice, as shown in Fig. 3. For the loading method I, the molecule first climbs the potential hill from position A_1 to B_1 , which is accompanied by a loss in kinetic energy.

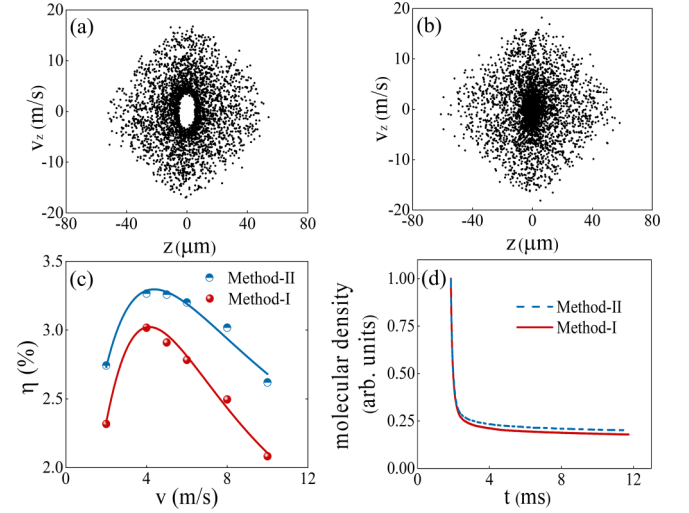


FIG. 4. The calculated longitudinal phase-space distribution of ND_3 molecules at $t = 2 \text{ ms}$ for the loading methods I (a) and II (b), respectively. (c) The loading efficiency of ND_3 molecules as a function of the forward velocity using two different loading schemes. (d) The dependence of the molecular number density upon a time in the lattice sites for different loading methods.

Then the molecule continues to fly freely to the following lattice site minimum and repeats the above slowing process until at a standstill. For the loading method II, the synchronous molecule is first decelerated from position A_2 to B_2 and then the electric field configuration (dotted blue curves) is switched to another one (dashed red curves), where the minimum of the trap exactly overlaps the position of the synchronous molecule. This is achieved by suitably choosing the voltages on the lattice plates. In principle, the lattice enables constructing electric field configurations with the trap minima at any position.

To verify the feasibility of these loading methods, 3D numerical calculations are carried out using ND_3 molecules in the $|J, KM\rangle = |1, -1\rangle$ state as a tester. In the following simulations, the molecular losses due to background collisions and nonadiabatic transition are not considered in our calculations [29,30], and molecules hitting the surface of the electrode are eliminated. Both the position and the velocity distribution of the ND_3 molecular beam is flat in any direction with the six-dimensional (6D) emittance $[500 \mu\text{m} \times 2 \text{ m/s}] \times [500 \mu\text{m} \times 2 \text{ m/s}] \times [500 \mu\text{m} \times 2 \text{ m/s}]$ (in the x , y , and z axis, respectively). The molecular beam contains 7×10^6 molecules with an initial distribution centered at $x = 30 \mu\text{m}$, $v_x = 0 \text{ m/s}$, $y = 30 \mu\text{m}$, $v_y = 0 \text{ m/s}$, $z = 0 \mu\text{m}$, and $v_z = 4 \text{ m/s}$. The above parameters of the tailored molecular beam are chosen by referring to the related experimental parameters [31]. In the calculation, the transverse dimension of the lattice is set to $7 \text{ mm} \times 7 \text{ mm}$, and the longitudinal dimension is about 10 mm . The starting position of the trajectory is the end of the hexapole downstream from the Stark decelerator, which is 2 mm away from the 3D lattice. The voltage of the lattice V_0 is set to 100 V , and the trap depth in the longitudinal direction reaches 0.2 cm^{-1} , allowing for confining ND_3 molecules with a maximum velocity of approximately 15 m/s . Figure 4 shows the calculated results in only one lattice site.

Figures 4(a) and 4(b) depict the longitudinal phase-space distributions of ND_3 molecules after 2 ms using the loading methods I and II, respectively. In Fig. 4(a), the phase-space distribution in the lattice is characteristic of an empty center, which arises from the defective match between the molecular packets and the acceptance of the potential traps, namely, the center of the molecular packet deviates from the center of the potential wells when the traps are switched on. In loading method II, the beam center matches well with the trap center, and thus most molecules can occupy the trap center stably. Figure 4(c) shows the loading efficiency of the lattice as a function of the forward velocity via two different methods. The loading efficiency refers to the ratio between the confined molecules in the lattice and the original molecules. When the forward velocity is ~ 4 m/s, the optimum loading efficiency of the 3D lattice using the first method is estimated to be about 3%. Compared to the first method, the second loading strategy slightly improves the loading efficiency at any velocity, with the optimum loading efficiency increased to 3.3% when $v_z = 4.0$ m/s. Figure 4(d) depicts the molecular density dependence on time using two different loading methods, which indicates that both permit stable confinement for ND_3 molecules.

B. Evaporative cooling

Scientists have realized low-entropy quantum gases of polar molecules via the synthetic method in 3D optical lattices [32], which inhibits chemical reactions between molecules. A filling fraction of 25%–30% is obtained in their experiments, limited by the molecular preparation efficiency. A larger filling fraction means lower entropy per particle in a lattice, which in principle could be achieved for natural molecules via various ways like adiabatic cooling, Sisyphus cooling, or evaporative cooling of trapped molecules. These cooling methods have been demonstrated in a single electric trap. Here, we utilize the Monte Carlo simulation approach to study the production of a low-entropy gas of polar molecules in our designed 3D electric lattice through evaporative cooling.

Evaporative cooling in our 3D electric lattice is performed by ramping down the voltages on the electrodes, thus lowering the potential depth of the lattice sites and removing the hottest molecules. In our Monte Carlo simulations, the voltages applied on the 3D lattice are slowly changed from 100 to 10 V in 1 ms and kept for 2 ms. Following that, the voltages are gradually increased back to 100 V in 1 ms and kept for 5 ms. It is worth noting that during the evaporative cooling process, the ramping time should be sufficiently long for molecules to follow the change in potential, that is, $dT/dt \ll 1$ [33], where dT and dt represent the trapping period and ramping time, respectively. The trap frequency of the 3D lattice site is $f = 97$ and 31 kHz when the applied voltage is 100 and 10 V, respectively. When the voltages are reduced from 100 to 10 V, the trapping period is varied from 10 to 33 μs , both of which are much less than the ramping time $\Delta t = 1$ ms, and therefore satisfy the cooling conditions.

In current simulations, the initial molecular packet contains 6×10^6 molecules and has a 6D emittance [$200 \mu\text{m} \times 6 \text{ m/s}$] \times [$200 \mu\text{m} \times 6 \text{ m/s}$] \times [$500 \mu\text{m} \times 16 \text{ m/s}$] (in the x , y , and z axis, respectively). The packet distribution is

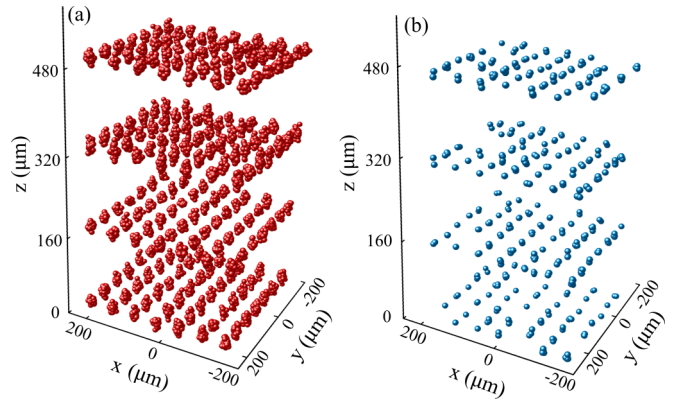


FIG. 5. Space-periodic ND_3 molecular packets in the 3D electrostatic lattice at voltages of 100 V (a) and 40 V (b).

centered at $x = 30 \mu\text{m}$, $v_x = 0$ m/s, $y = 30 \mu\text{m}$, $v_y = 0$ m/s, $z = 250 \mu\text{m}$, and $v_z = 0$ m/s. The potential-well depth in the z direction is about 0.19 cm^{-1} , which can confine the molecules to less than 15 m/s. The potential depth in the $x(y)$ direction is much shallower than the longitudinal one, reaching 0.02 cm^{-1} , thus allowing molecules below 5 m/s to oscillate in the trap. Figure 5(a) shows the spatial distribution of molecules confined in the lattice after about 10 ms with $V_0 = 100$ V. It is clear that arrays of molecular packets are formed in 3D space and the temperature of the molecular packets in the lattice is 24 mK. Now we start evaporative cooling from $V_0 = 100$ V. As the voltage of the lattice decreases, the trap depth becomes shallower and the hottest molecules escape from potential wells. Figure 5(b) shows the calculated results of the 3D spatial distribution of ND_3 molecules in the lattice with $V_0 = 40$ V. The temperature of the molecular packets in the lattice is reduced from 24 to 13 mK as the voltages lower from 100 to 40 V. The temperature of the packet can be obtained from $(3/2)k_B T = (1/2)k_B T_L + k_B T_T$ [34], where T_L and T_T are the corresponding longitudinal and transverse temperatures of the molecular packets and are given by $T_{x,y,z} = m \Delta v_{x,y,z}^2 / 8 \ln 2 k_B$ [35], where k_B is Boltzmann constant, m denotes the mass of the molecule, and $\Delta v_{x,y,z}$ is the velocity spread of the molecular packet. Note

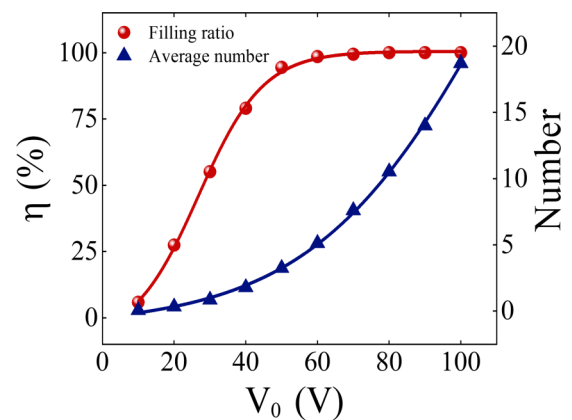


FIG. 6. The dependence of the filling ratio and the average number of molecules per lattice site on applied electrode voltage, respectively.

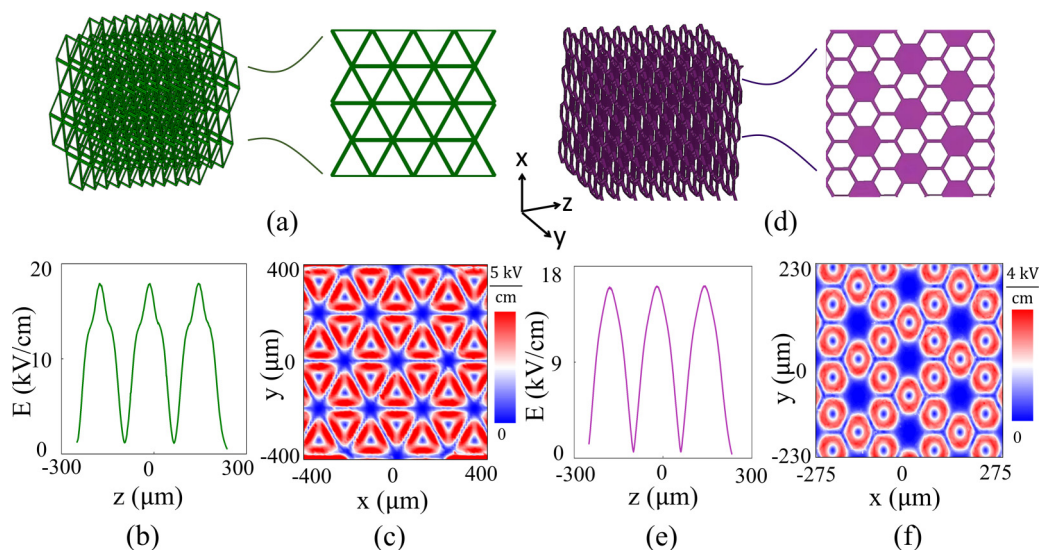


FIG. 7. The design of hexagonal honeycomb (a) and kagome (d) 3D electric lattices and the pattern in the electrodes. Electric field distribution of the honeycomb (b) and the kagome lattices (e) along the z direction. The two-dimensional transverse electric field distributions through the lattice site minima of the honeycomb (c) and the kagome (f) 3D lattices, together with the electric field strength bar.

that within our evaporative cooling timescale, the densities in the lattice are too low to have thermalization, and the concept of temperature used here is only for the convenience to represent the molecular distribution. Figure 6 shows the filling ratio of the lattice that is reduced from 100% to about

6% when the voltages decrease from 100 to 10 V. Here, the filling ratio refers to the number of occupied lattice sites to the total number of sites. Simultaneously, the average molecular number per lattice is lowered from 19 to 0.06, also as shown in Fig. 6.

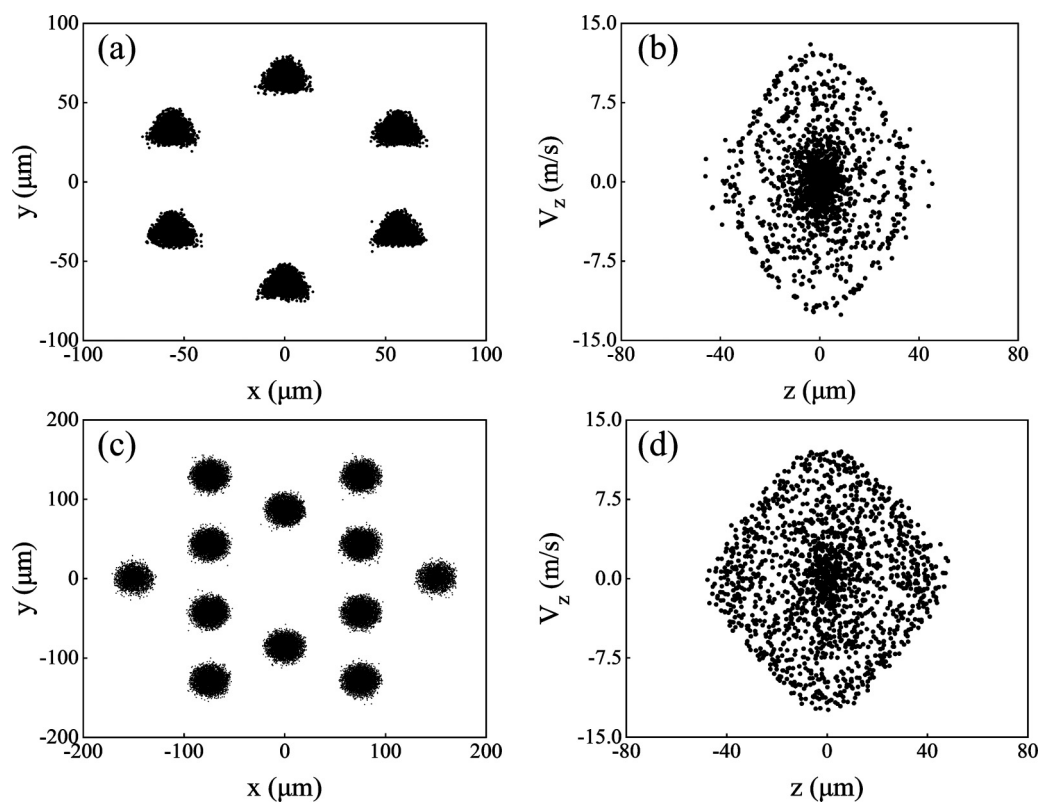


FIG. 8. Transverse space distribution of ND_3 molecules in the honeycomb (a) and the kagome (c) lattices after 2 ms of confinement. Molecular phase-space distribution in the z direction in the honeycomb (b) and the kagome (d) lattice sites.

IV. OTHER TOPOLOGICAL 3D ELECTROSTATIC LATTICES

Topology has emerged in the last few decades and played a pivotal role in the search for novel phases of matter. Tremendous efforts have been devoted to exploring novel topological phases of material since the discovery of the quantum Hall effect and topological insulators [36–38]. Ultracold atomic and molecular gases stored in the optical lattice offer a unique platform for the implementation of exotic topological states and band structures.

The geometry of an optical lattice can be controlled by changing the angles of the interference lasers [39]. Analogous to the optical and magnetic lattices, our 3D electrostatic lattice can be constructed with the flexibility of transforming the 3D lattice to various topological geometries via changing the pattern in the plates. Figure 7(a) depicts our designed honeycomb 3D electric lattice, which is formed by an array of electrodes in a triangular pattern. Figures 7(b) and 7(c) present the longitudinal and the transverse electric field distributions through the lattice site minima, respectively. We can imagine that an array of true 3D electrostatic traps characteristic of honeycomb geometry could be formed for polar molecules in low-field-seeking states. Similarly, various topological 3D electric lattices such as kagome and triangular lattices can also be generated. Figures 7(d)–7(f) show the construction of the 3D electric kagome lattice, including the pattern in the electrodes and corresponding electric field distributions. Kagome lattice is thought to possess many essential features of high-temperature superconductors [40].

With similar parameters of the molecular beam, we carried out the numerical simulations for trapping ND_3 molecules in both the honeycomb and the kagome lattices. Figures 8(a) and 8(c) depict the transverse distribution of ND_3 molecules after trapping 2 ms in the lattice. Figures 8(b) and 8(d) illustrate the molecular phase-space distribution in one site. These results show the possibility of the honeycomb and kagome electric lattice schemes.

V. CONCLUSION

We have proposed a scheme of 3D electrostatic lattice suitable for cooling and controlling polar molecules in the low-field-seeking states, whose lattice formed by periodical

electrodes offers a high degree of design flexibility. The depth of the lattice and the local electric field distribution can be easily tweaked by changing the voltages on the electrodes. Theoretical analysis and Monte Carlo simulations have been carried out to justify the possibility of our scheme. Combined with laser polarization gradient cooling, the 3D lattice might further cool molecules to ultracold temperatures [41], thus paving the way for the development of controlled cold chemistry, quantum simulation, and quantum metrology. By changing the pattern in the electrode plates, the 3D electric lattice can generate numerous complex landscapes for polar molecules, such as hexagonal, triangular, and kagome lattices, which facilitate engineering many-body systems to realize and probe exotic topological phenomena.

The lattice constant of the 3D electric lattice presented here is about two orders of magnitude larger than the 3D optical lattice, which is too long to study many-body systems using polar molecules. From the point of view of processing feasibility, reducing the geometry of the 3D electric lattice by one order of magnitude or more could be enabled by modern micro-nano structure processing technology [42,43]. When scaled down, our 3D electric lattice may apply to polar molecules with the largest electric dipole moments. From the perspective of easier implementation, the 3D electric lattice may be more suitable for exotic particles, such as Rydberg atoms with extremely large electric dipole moments [44], between which the interaction distance can approach the scale of tens of micrometers [45] with considerable interaction up to tens of kilohertz. The highly tailored and well-controlled 3D electric lattice provides a natural stable platform for a full 3D gas of polar molecules and adds new elements to the toolbox for engineering many-body systems.

ACKNOWLEDGMENTS

This work is supported by the National Natural Science Foundation of China (Grants No. 11834003, No. 91536218, and No. 11874151), the Fundamental Research Funds for the Central Universities, the Program for Professor of Special Appointment (Eastern Scholar) at Shanghai Institutions of Higher Learning, and the Young Top-Notch Talent Support Program of Shanghai.

-
- [1] D. Jaksch, C. Bruder, J. I. Cirac, C. W. Gardiner, and P. Zoller, *Phys. Rev. Lett.* **81**, 3108 (1998).
 - [2] M. Greiner, O. Mandel, T. Esslinger, T. W. Hänsch, and I. Bloch, *Nature (London)* **415**, 39 (2002).
 - [3] I. Bloch, *Nat. Phys.* **1**, 23 (2005).
 - [4] G. Grynberg and J.-Y. Courtois, *Europhys. Lett.* **27**, 41 (1994).
 - [5] A. Günther, S. Kraft, M. Kemmler, D. Koelle, R. Kleiner, C. Zimmermann, and J. Fortágh, *Phys. Rev. Lett.* **95**, 170405 (2005).
 - [6] S. Ghanbari, P. B. Blakie, P. Hannaford, and T. D. Kieu, *Eur. Phys. J. B* **70**, 305 (2009).
 - [7] H. L. Bethlem, G. Berden, and G. Meijer, *Phys. Rev. Lett.* **83**, 1558 (1999).
 - [8] J. R. Bochinski, E. R. Hudson, H. J. Lewandowski, G. Meijer, and J. Ye, *Phys. Rev. Lett.* **91**, 243001 (2003).
 - [9] A. Osterwalder, S. A. Meek, G. Hammer, H. Haak, and G. Meijer, *Phys. Rev. A* **81**, 051401(R) (2010).
 - [10] E. Narevicius, A. Libson, C. G. Parthey, I. Chavez, J. Narevicius, U. Even, and M. G. Raizen, *Phys. Rev. Lett.* **100**, 093003 (2008).
 - [11] S. D. Hogan, A. W. Wiederkehr, M. Andrist, H. Schmutz, and F. Merkt, *J. Phys. B: At., Mol. Opt. Phys.* **41**, 081005 (2008).
 - [12] R. Fulton, A. I. Bishop, and P. F. Barker, *Phys. Rev. Lett.* **93**, 243004 (2004).
 - [13] E. S. Shuman, J. F. Barry, and D. DeMille, *Nature (London)* **467**, 820 (2010).

- [14] J.-R. Li, W. G. Tobias, K. Matsuda, C. Miller, G. Valtolina, L. De Marco, R. R. W. Wang, L. Lassablière, G. Quéméner, J. L. Bohn, and J. Ye, *Nat. Phys.* **17**, 1144 (2021).
- [15] A. O. G. Wallis and J. M. Hutson, *Phys. Rev. Lett.* **103**, 183201 (2009).
- [16] S. Truppe, M. Hambach, S. Skoff, N. Bulleid, J. Bumby, R. Hendricks, E. Hinds, B. Sauer, and M. Tarbutt, *J. Mod. Opt.* **65**, 648 (2018).
- [17] C. A. Regal, C. Ticknor, J. L. Bohn, and D. S. Jin, *Nature (London)* **424**, 47 (2003).
- [18] S. Jochim, M. Bartenstein, A. Altmeyer, G. Hendl, S. Riedl, C. Chin, J. Hecker Denschlag, and R. Grimm, *Science* **302**, 2101 (2003).
- [19] P. D. Lett, K. Helmerson, W. D. Phillips, L. P. Ratliff, S. L. Rolston, and M. E. Wagshul, *Phys. Rev. Lett.* **71**, 2200 (1993).
- [20] J. D. Miller, R. A. Cline, and D. J. Heinzen, *Phys. Rev. Lett.* **71**, 2204 (1993).
- [21] S. A. Meek, H. L. Bethlem, H. Conrad, and G. Meijer, *Phys. Rev. Lett.* **100**, 153003 (2008).
- [22] S. A. Meek, H. Conrad, and G. Meijer, *Science* **324**, 1699 (2009).
- [23] S. Hou, B. Wei, L. Deng, and J. Yin, *Phys. Rev. A* **96**, 063416 (2017).
- [24] B. Wei, H. Guo, Y. Ji, T. Yang, S. Hou, and J. Yin, *Opt. Commun.* **475**, 126208 (2020).
- [25] Q. Wang, S. Hou, L. Xu, and J. Yin, *Phys. Chem. Chem. Phys.* **18**, 5432 (2016).
- [26] C. E. Otis and P. M. Johnson, *Rev. Sci. Instrum.* **51**, 1128 (1980).
- [27] U. Even, *EPJ Tech. Instrum.* **2**, 17 (2015).
- [28] S. A. Meek, Ph.D. thesis, Freie Universität, 2010.
- [29] S. Y. Buhmann, M. R. Tarbutt, S. Scheel, and E. A. Hinds, *Phys. Rev. A* **78**, 052901 (2008).
- [30] S. A. Meek, G. Santambrogio, B. G. Sartakov, H. Conrad, and G. Meijer, *Phys. Rev. A* **83**, 033413 (2011).
- [31] F. M. H. Crompvoets, R. T. Jongma, H. L. Bethlem, A. J. A. van Roij, and G. Meijer, *Phys. Rev. Lett.* **89**, 093004 (2002).
- [32] S. A. Moses, J. P. Covey, M. T. Miecnikowski, B. Yan, B. Gadway, J. Ye, and D. S. Jin, *Science* **350**, 659 (2015).
- [33] L. D. Landau and E. M. Lifshitz, *Mechanics*, 3rd ed. (Butterworth-Heinemann, Oxford, 1993), Vol. 1.
- [34] *Atomic and Molecular Beam Methods*, edited by G. Scoles (Oxford University Press, New York, 1986), p. 27.
- [35] M. Gupta and D. Herschbach, *J. Phys. Chem. A* **103**, 10670 (1999).
- [36] E. Haller, J. Hudson, A. Kelly, D. A. Cotta, B. Peaudecerf, G. D. Bruce, and S. Kuhr, *Nat. Phys.* **11**, 738 (2015).
- [37] M. F. Parsons, F. Huber, A. Mazurenko, C. S. Chiu, W. Setiawan, K. Wooley-Brown, S. Blatt, and M. Greiner, *Phys. Rev. Lett.* **114**, 213002 (2015).
- [38] L. W. Cheuk, M. A. Nichols, M. Okan, T. Gersdorf, V. V. Ramasesh, W. S. Bakr, T. Lompe, and M. W. Zwierlein, *Phys. Rev. Lett.* **114**, 193001 (2015).
- [39] G.-B. Jo, J. Guzman, C. K. Thomas, P. Hosur, A. Vishwanath, and D. M. Stamper-Kurn, *Phys. Rev. Lett.* **108**, 045305 (2012).
- [40] C. Peng, Y. F. Jiang, D. N. Sheng, and H. C. Jiang, *Adv. Quantum Technol.* **4**, 2000126 (2021).
- [41] K. Yan, B. Wei, Y. Yin, S. Xu, L. Xu, M. Xia, R. Gu, Y. Xia, and J. Yin, *New J. Phys.* **22**, 033003 (2020).
- [42] Y.-L. Zhang, Q.-D. Chen, H. Xia, and H.-B. Sun, *Nano Today* **5**, 435 (2010).
- [43] M. Malinauskas, A. Žukauskas, S. Hasegawa, Y. Hayasaki, V. Mizeikis, R. Buividas, and S. Juodkazis, *Light Sci. Appl.* **5**, e16133 (2016).
- [44] A. Browaeys and T. Lahaye, *Nat. Phys.* **16**, 132 (2020).
- [45] D. Barredo, V. Lienhard, P. Scholl, S. de Léséleuc, T. Boulier, A. Browaeys, and T. Lahaye, *Phys. Rev. Lett.* **124**, 023201 (2020).